# Automated Machine Learning Framework for Generating Pseudorandom Antenna Designs Conditioned on Operational Frequency Range

Bartosz Czaplewski [1,[0000-0001-7904-5567]], Tom Dhaene [2,[0000-0003-2899-4636]]

[1] Department of Teleinformation Networks, Faculty of Electronics, Telecommunications and Informatics, Gdansk University of Technology, Narutowicza 11/12, 80-233 Gdansk, Poland
[2] Department of Information Technology (INTEC), IDLab, Ghent University-imec, iGent, Technologiepark-Zwijnaarde 126, 9052 Ghent, Belgium
bartosz.czaplewski@pg.edu.pl

**Abstract.** This paper presents a fully automated machine learning framework for generating high-complexity, free-form planar antenna designs conditioned on a specified operational frequency range. The proposed system eliminates human engineer bias by combining generative and predictive neural networks into an end-to-end antenna design pipeline. Its core component is a conditional variational autoencoder (CVAE) that produces pseudorandom yet physically feasible antenna geometries guided by frequency-band labels. Three latent-space sampling strategies—posterior, linear interpolation, and convex interpolation—are explored to balance design diversity and conditional consistency. Auxiliary models implemented as multilayer perceptrons (MLPs) and a convolutional neural network (CNN) perform iterative verification of generated structures, including viability detection, label classification, and reflection response estimation, without the need for costly full-wave electromagnetic simulations. The framework is trained and validated using two large-scale datasets of pseudo-random antennas—1DDesign-to-Label-1.8.3 and 1DDesign-to-Response-2.8—comprising a total of over 320,000 geometries with corresponding performance labels and reflection responses. Experimental validation using independent CST Microwave Studio simulations demonstrates that the best model achieves an exact-match accuracy of 0.634, a relaxed-match accuracy of 0.769, a macro-average accuracy of 0.947, and a macro-average F1 score of 0.756. The average generation and verification time per design is 0.703 s. The proposed approach enables rapid, bias-free antenna design exploration and candidate preselection, significantly reducing design time as well as dependence on expert knowledge and EM computation. The framework's modular structure allows further enhancement, making it a versatile foundation for next-generation computer-aided antenna engineering.

**Keywords:** Machine Learning; Conditional Variational Autoencoder; Neural Networks; Antenna Design Generation; Automated Antenna Engineering.

ICCS Camera Ready Version 2026
To cite this paper please use the final published version:
DOI: 10.1007/978-3-032-29921-5_8

## 1 Introduction

Wireless communication enables the exchange of information through electromagnetic waves and forms the basis modern communication technologies. Consequently, antenna design remains a critical research area, especially under modern requirements of miniaturization, multiband operation, and frequency reconfigurability.

Conventional antenna design is an iterative, experience-driven process comprising substrate selection, geometry formulation, and parametric tuning. Although effective, this approach is limited by engineering bias—the designer's reliance on familiar shapes and heuristics developed through experience [1, 2]. Such bias constrains topological diversity and may overlook unconventional yet high-performance geometries.

Automation has emerged to mitigate bias and accelerate development. Optimization-based design enables antenna topologies to evolve from performance specifications rather than predefined forms [3–6]. Yet, despite their flexibility, these algorithms often incur high computational costs due to numerous electromagnetic (EM) simulations. This motivates the search for data-efficient strategies for early-stage antenna geometry exploration, where maintaining diversity and feasibility is crucial.

Such automation demands free-form geometric representations, modeled in two ways [4–6]: as assemblies of primitive shapes [7–10] or as sets of coordinate points [11–14]. The shape-based approach uses binary matrices to define conductive elements, while the point-based approach connects nodes via lines or splines. In both cases, free-form designs require many parameters for topological flexibility, causing high computational cost from EM simulations. Their multimodal nature makes simulation-driven optimization, such as population-based metaheuristics, impractical [11, 12, 15, 16]. Surrogate-assisted search can reduce this cost [11, 17], but relies on good initial designs, highlighting the need for automated, bias-free generation [18–21].

Machine learning (ML) enables data-driven modeling and optimization across domains, including cybersecurity [22–24], 5G management [25–27], and antenna design [28, 29]. Recent studies show that ML can predict antenna behavior, aid shape synthesis, and support optimization. Yet, most methods refine predefined or parametric designs, offering limited support for early-stage exploration. Hence, there is a need for ML-based tools that can identify promising antenna topologies from scratch.

The goal of this research is to develop a fully automated ML framework for generating high-complexity free-form planar antenna designs tailored to a target operational frequency range. The system integrates generative, classification, and regression models to create and verify feasible designs without dependence on expert knowledge or repetitive EM simulations, providing initial geometries for subsequent optimization. The main contributions include: (1) an end-to-end ML-based framework for automated free-form antenna design; (2) a conditional variational autoencoder (CVAE) for label-driven geometry synthesis; (3) the integration of auxiliary ML models for iterative verification; and (4) a comprehensive performance assessment.

Section 2 reviews related work. Section 3 outlines the methodology. Section 4 describes the datasets. Sections 5–9 detail the components of the framework: latent sampling, design generator, viability detector, label classifier, and response estimator. Section 10 presents results, and Section 11 concludes.

ICCS Camera Ready Version 2026
To cite this paper please use the final published version:
DOI: 10.1007/978-3-032-29921-5_8

## 2 Related Work

No prior work presents an ML-based method for automatic and conditioned generation of complex free-form antenna designs, without expert knowledge or EM simulations. Related studies address (1) parameter synthesis, (2) resonant frequency prediction, (3) reflection estimation, (4) antenna classification.

In the parameter synthesis group, work [30] introduced a synthesis framework that first classifies antenna type based on desired electromagnetic characteristics and then predicts geometry using ensemble learning. Research [31] followed a similar concept, combining decision tree classification with fuzzy inference for geometric prediction. These methods are limited to predefined low-complexity antennas, constraining design exploration and preventing discovery of unconventional geometries.

In the resonant frequency prediction group, study [9] used a convolutional neural network (CNN) to predict frequencies of pixelated microstrip antennas from binary geometry matrices, enabling more complex shapes yet limited to dual-band designs. Research [32] introduced a semi-supervised co-training approach combining Gaussian processes and support vector machines (SVM) to predict resonant frequencies and reflection responses from few samples, but limited to simple antennas. Work [33] used a CNN on binary-encoded geometric data of rectangular antennas, aiming for a surrogate model yet relying on symbolic rather than spatial input.

In the reflection response estimation group, study [34] used a progressive Gaussian process to model $|S_{11}|$ for simple monopoles, producing pointwise predictions over multiple frequencies with iterative sample selection, yet the study remained limited to low-complexity antennas and small datasets. Work [35] combined CNN and particle swarm optimization to predict reflection samples of pixelated antennas, achieving higher complexity but relying on visual validation rather than quantitative metrics.

In the antenna classification group, study [36] uses deep CNNs, such as LeNet and ResNet, for selecting optimal receive antennas in multiple-input multiple-output (MIMO) systems to maximize channel capacity while reducing computational complexity. The CNN takes a normalized channel matrix as input and outputs a class label corresponding to the best antenna subset. Accuracy measures how often the CNN selects the optimal set. Research [37] classifies randomly generated microstrip antennas by potential operational frequency ranges using multi-label classification, without EM simulations or expert knowledge. The model predicts which of the ten sub-bands meet reflection and bandwidth criteria, allowing antennas to belong to multiple classes, and is compatible with the approach proposed here.

## 3 Methodology

Fig.1. shows the proposed pseudorandom microstrip antenna generator. The goal is to fully automate antenna design, eliminating human bias and yielding candidates for further tuning. The generated topology is constrained to operate within a target frequency range. A design qualifies as a candidate if, within this range, the reflection coefficient is below $\theta_R = -3$ dB, and the relative bandwidth exceeds $\theta_W = 0.1$.

ICCS Camera Ready Version 2026
To cite this paper please use the final published version:
DOI: 10.1007/978-3-032-29921-5_8

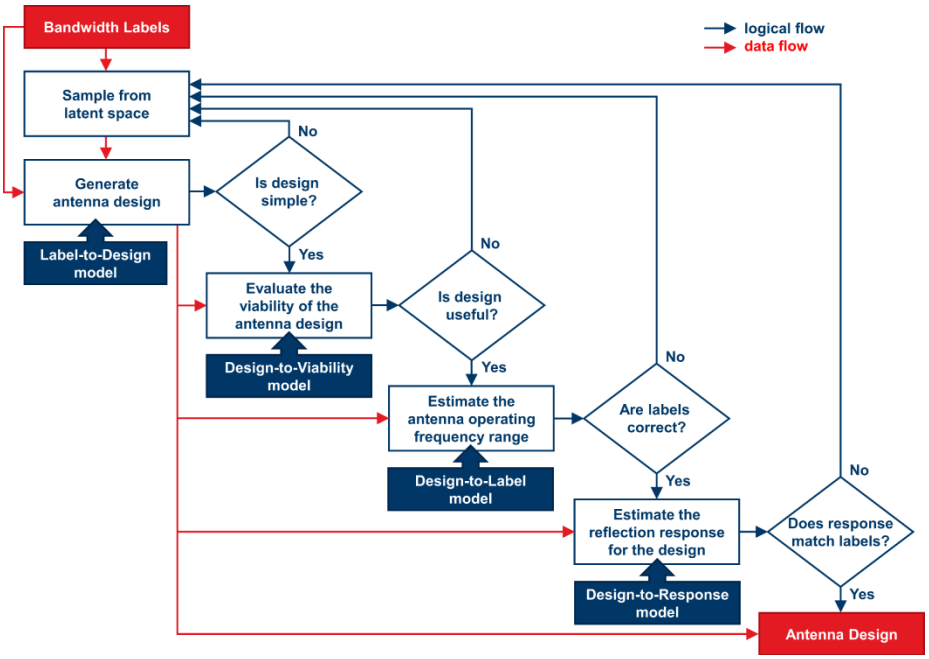


**Fig. 1.** Overall workflow of the proposed antenna design generator.

The input is a 10-bit condition vector $\mathbf{B}=[b_g\in\{0,1\}]$, $b=1,\ldots,10$, where $b_g=1$ denotes antenna operation in the $g$-th 0.5 GHz sub-band within 3–8 GHz. The output is a 103-element design vector $\mathbf{D}^{(103)}=[\alpha,q_x,q_y,\mathbf{v}_x,\mathbf{v}_y]$, where $\alpha\in\langle 24,36\rangle$ is a scaling factor, $q_x$, $q_y$ are feed point coordinates, and $\mathbf{v}_x$, $\mathbf{v}_y$ are coordinates of 50 vertices ($\in<-1,+1>$). The physical dimensions (mm) are obtained by scaling: $\alpha\cdot[\mathbf{v}_x,\mathbf{v}_y]$ and $\alpha\cdot[q_x,q_y]$.

The overall generation and verification process consists of the following steps:

1. **Latent space sampling.** A latent vector is sampled from the CVAE latent space—a compact numerical representation of antenna designs, where geometric and EM relationships are encoded in a lower dimension. Operating in this space enables efficient exploration of the design domain, interpolation between known solutions, and generation of novel yet valid geometries. The latent sample is obtained to match the specified bandwidth labels (Section 5).
2. **Design generation.** The target bandwidth labels and the latent sample are fed into the Label-to-Design model (Section 6). This generative model uses only the CVAE decoder to produce a pseudorandom antenna design that approximately satisfies the specified condition. The output is a not-yet-evaluated structure requiring further assessment.
3. **Geometry check.** The generated design is verified to be a simple polygon, i.e. edges intersect only at endpoints, forming overlap-free surface. This property is crucial for planar antennas, as self-intersecting shapes are unrealizable and yield invalid simulations. If a design fails the check, the process restarts.

ICCS Camera Ready Version 2026
To cite this paper please use the final published version:
DOI: 10.1007/978-3-032-29921-5_8

4. **Viability check.** The design is evaluated using the Design-to-Viability model (Section 7), which performs binary classification to determine if it can operate in any 3–8 GHz sub-band. If a design is non-viable, the process restarts.
5. **Label consistency check.** The design is evaluated by the Design-to-Label model performing multi-label classification. The model outputs predicted bandwidth labels (Section 8). If the predicted labels do not match the input condition, the design is rejected and the process restarts.
6. **Reflection response check.** The design is evaluated by the Design-to-Response regression model, which predicts the full reflection response without EM simulation (Section 9). If the predicted response does not satisfy the target bandwidth condition, the process restarts; else, it is accepted as the output.

The above procedure constitutes a multi-stage evaluation mechanism, a key distinction from [37]. Instead of relying on a single classifier, the proposed framework uses a hierarchical verification pipeline combining geometric validation, binary viability detection, multi-label classification, and regression-based response estimation. Stages 3–6 act as a rejection filters, ensuring that only designs satisfying increasingly strict criteria are accepted. The models in these steps serve as fast surrogate filters guiding the generation process, not as final evaluators. Actual performance of generated designs is verified with full-wave EM simulations as ground truth (Section 10).

## 4 Datasets

The datasets used in this work consist of pseudo-randomly generated antenna designs. The term pseudorandom refers to a constrained random generation process used to construct antenna geometries. Radial distances and angular increments are sampled randomly within predefined ranges and further processed to enforce structural constraints. In particular, angular coordinates are accumulated and normalized to span the full 0–2π interval, ensuring an ordered contour and preventing self-intersections. This guarantees that each shape forms a continuous, closed loop without internal holes. The feed point is randomly assigned within the contour. The generated geometries are random in their local variations but globally structured, yielding physically valid antenna outlines. The geometry is then transformed into Cartesian coordinates.

The first dataset, 1Ddesign-to-Label-1.8.3 [38], contains 106,351 pseudorandom antenna designs labeled by which of the ten 0.5 GHz sub-bands within the 3–8 GHz satisfy both conditions (reflection coefficient $< \theta_R$, relative bandwidth $> \theta_W$), indicating suitability for further optimization. An example is shown in Fig. 2. The dataset also includes 105,000 unlabeled designs that do not meet the criteria in any sub-band.

ICCS Camera Ready Version 2026
To cite this paper please use the final published version:
DOI: 10.1007/978-3-032-29921-5_8

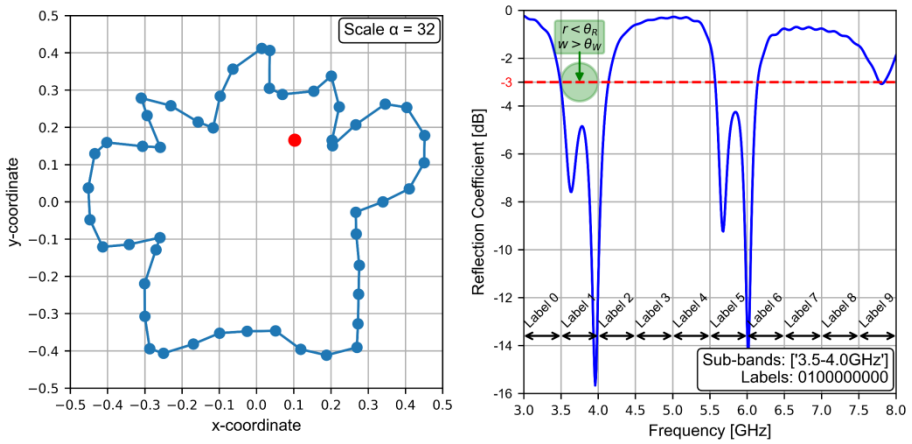


**Fig. 2.** Example of an antenna design with the corresponding reflection response and labels.

In the 1Ddesign-to-Label-1.8.3 dataset, each design is a 103-element vector: $\mathbf{D}^{(103)}=[\alpha,q_x,q_y,\mathbf{v}_x,\mathbf{v}_y]$, where $\alpha\in\langle 24,36\rangle$ is a scaling factor, $q_x$, $q_y$ are feed point coordinates, and $\mathbf{v}_x$, $\mathbf{v}_y$ are coordinates of 50 vertices ($\in<-1,+1>$). Physical dimensions (mm) are $\alpha\cdot[\mathbf{v}_x,\mathbf{v}_y]$ and $\alpha\cdot[q_x,q_y]$. Labels are a 10-element vector: $\mathbf{B}=[b_g\in\{0,1\}]$, where $b_g=1$ denotes operation in the $g$-th 0.5 GHz sub-band within 3–8 GHz.

To assign labels, reflection responses were computed for 20,000 designs with $\alpha=30$ using CST Microwave Studio [39], based on the Finite Integration Technique [4–6]. Responses for other $\alpha$ values were obtained by frequency scaling [17]. Each design was labeled if its reflection coefficient fell below $\theta_R$ within a frequency region whose relative bandwidth exceeded $\theta_W$, matching predefined sub-bands. As antennas may operate in multiple bands, this forms a multi-label problem [37].

The 1Ddesign-to-Label-1.8.3 dataset was used to train the Label-to-Design, Design-to-Label, and Design-to-Viability models. For each model, the designs were normalized to the range <0,1>, with $\alpha$ scaled separately from the coordinates.

The Design-to-Viability model was trained on the entire dataset, including both labeled and unlabeled samples, to perform binary classification of viable vs. non-viable designs. The Design-to-Label model used only labeled samples, assuming that inputs were already verified as viable, which improved label prediction accuracy and avoided influence from non-functional designs. The Label-to-Design model was likewise trained only on labeled samples, as it generates new designs. Excluding unlabeled data ensured learning from meaningful structures and improved generation success.

The second dataset, 1Ddesign-to-Response-2.8 [40], comprises 108,710 pseudorandom free-form antenna designs with corresponding EM simulated reflection response. All geometries were simulated in CST Microwave Studio using the Finite Integration Technique. In this dataset, a full simulation was performed for each design without data augmentation via frequency scaling. An example is shown in Fig. 2.

In the 1Ddesign-to-Response-2.8 dataset, each design is a 102-element vector $\mathbf{D}^{(102)}=[q_x,\mathbf{v}_x,q_y,\mathbf{v}_y]$, where $q_x$, $q_y$ are the feed point coordinates, and $\mathbf{v}_x=[v_{x1},\ldots,v_{x50}]$,

ICCS Camera Ready Version 2026
To cite this paper please use the final published version:
DOI: 10.1007/978-3-032-29921-5_8

$\mathbf{v}_y=[v_{y1},\ldots,v_{y50}]$ define 50 vertex positions in the xy-plane. All coordinates range from –20 to +20 mm, matching the physical antenna size, with no scaling factor α applied. The reflection response is a 251-element vector of $S_{11}(f)$ (dB), i.e., the return loss $20\cdot\log_{10}|S_{11}(f)|$, sampled over the 3-8 GHz range with a 20 MHz sampling step.

This dataset trained the Design-to-Response model, which predicts the reflection response as the final verification stage. Each 102-element vector was reshaped into a 2×51 tensor of x- and y-coordinates, with both channels standardized (z-score) independently. The response was also standardized but per frequency component. Standardization used statistics only from the training set to prevent data leakage.

## 5 Latent Sampler

Sampling in CVAEs draws latent vectors from a learned continuous space, creating compact representations of data. Proper sampling enables efficient exploration, interpolation between known samples, and generation of novel yet realistic outputs.

Latent vectors $z$ can be sampled from the posterior $q(z|x,y)$, where $x$ is the design, $y$ its labels. The encoder outputs the mean μ and log-variance $\log\sigma^2$, defining a Gaussian distribution in latent space. Then, μ and $\log\sigma^2$ are taken from a sample matching the condition labels, and $z$ is drawn as $z\sim N(\mu,\exp(0.5\cdot\log\sigma^2))$, ensuring the latent sample reflects features matching the conditions.

Next sampling strategy is interpolation-based generation of new latent vectors from two posterior samples. Two examples meeting the target bandwidth are encoded as $z_1$ and $z_2$ from $q(z|x_1,y)$ and $q(z|x_2,y)$. A new sample is generated via linear interpolation as $z=\lambda\cdot z_1+(1-\lambda)\cdot z_2$, $\lambda\in(0,1)$, exploring intermediate latent-space regions and blending features from both references while preserving smooth transitions and diversity.

The third sampling method extends interpolation to three posterior samples. Three designs meeting the bandwidth constraints are encoded as $z_1$, $z_2$, $z_3$ from their respective posterior distributions. A new latent vector is generated using a convex interpolation as $z=a\cdot z_1+b\cdot z_2+c\cdot z_3$, $a+b+c=1$, $a,b,c>0$, with coefficients drawn from a Dirichlet distribution. This method explores a wider latent-space region, increasing diversity while preserving structural consistency and physical plausibility.

## 6 Design Generator

The Label-to-Design model is a CVAE for antenna design reconstruction. It takes a design vector as input and a bandwidth label as condition (Fig. 3). The condition is projected to match the input and latent vector sizes and concatenated with them before the encoder and decoder, respectively, ensuring effective conditioning and stable generation. The model outputs a design consistent with the condition, meaning its predicted properties match the specified label. In the overall pipeline, only the decoder is used to generate new designs from latent samples and condition vectors.

The loss function $L=L_{REC}+\beta\cdot L_{KL}+\gamma\cdot L_{CONS}$ combines the reconstruction loss, the Kullback–Leibler divergence, and the consistency term. $L_{REC}$ is the Mean Squared Error (MSE) between the input and the reconstructed design, ensuring accurate recov-

ICCS Camera Ready Version 2026
To cite this paper please use the final published version:
DOI: 10.1007/978-3-032-29921-5_8

ery. $L_{KL}$ measures the difference between the posterior $q(z|x,y)$ and the prior $p(z)$. Scaling by $\beta$ promotes alignment with N(0,I) and better disentanglement in the latent space. $L_{CONS}$ enforces coherence between the reconstructed design and the condition, computed as Binary Cross-Entropy (BCE) between the true and predicted conditions from the auxiliary models. Scaling by $\gamma$ controls this constraint's strength.

The 1Ddesign-to-Label-1.8.3 dataset (Section 4) was split into 90% training and 10% test sets. A 10-fold cross-validation (CV) was performed, and the model with the lowest validation loss was evaluated on the test set. Hyperparameters were tuned via grid search. Architecture details are in Fig. 3, and learning parameters are in Table 1.

The model achieved a test loss of 0.002, indicating a highly effective balance between reconstruction quality, a well-structured latent space, and condition consistency. Consistency accuracy on the test set was measured by predicting bandwidth labels of generated designs using auxiliary models and comparing them with conditioning labels. Per-label consistency test accuracies ranged from 0.916 to 0.986, decreasing with increasing frequency. The consistency macro-average test accuracy was 0.964.

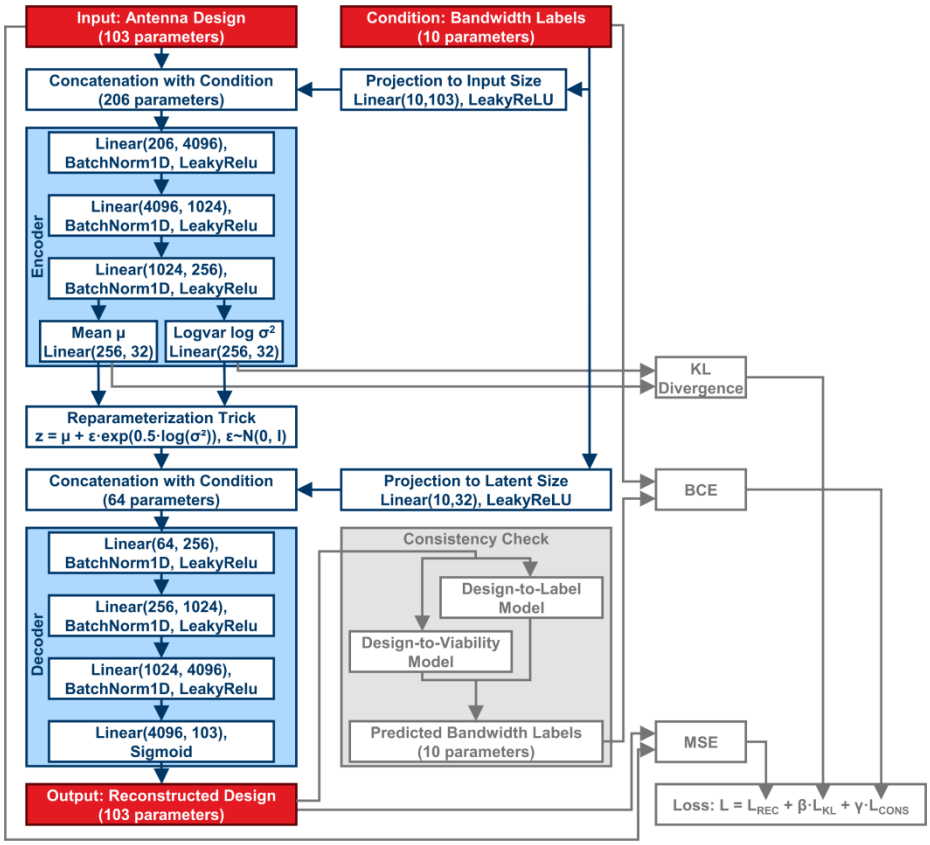


**Fig. 3.** Architecture of the Label-to-Design model.

ICCS Camera Ready Version 2026
To cite this paper please use the final published version:
DOI: 10.1007/978-3-032-29921-5_8

**Table 1.** Learning parameters used for all models.

| Parameter | Label-to-Design | Design-to-Viability | Design-to-Label | Design-to-Response |
|---|---|---|---|---|
| Solving algorithm | Adam | Adam | Adam | Adam |
| Learning rate (LR) | 1e-3 | 1e-3 | 1e-3 | 5e-4 |
| LR scheduler factor | 0.1 | 0.1 | 0.1 | 0.1 |
| LR scheduler patience | 5 | 5 | 5 | 5 |
| Weight decay (L2) | 0 | 1e-7 | 1e-7 | 1e-4 |
| Loss function | $L_{REC}+\beta \cdot L_{KL}+\gamma \cdot L_{CONS}$ | BCE | BCE | MSE |
| $\beta$ factor | 7.5e-6 | N/A | N/A | N/A |
| $\gamma$ factor | 1e-3 | N/A | N/A | N/A |
| Batch size | 64 | 64 | 64 | 64 |
| Early stopping | 15 | 15 | 10 | 10 |
| Number of parameters | 10,245,236 | 15,112,193 | 129,327,626 | 70,663,419 |

## 7 Viability Detector

The Design-to-Viability model is a MLP for detecting antenna design viability. It takes a design vector as input and outputs a binary result distinguishing viable from nonviable designs. An antenna design is considered viable if the reflection coefficient is below threshold $\theta_R$ and the relative bandwidth exceeds $\theta_W$, within any sub-band of the analyzed frequency range. In the workflow (Section 3), this model is used in step four to assess whether generated designs meet required criteria.

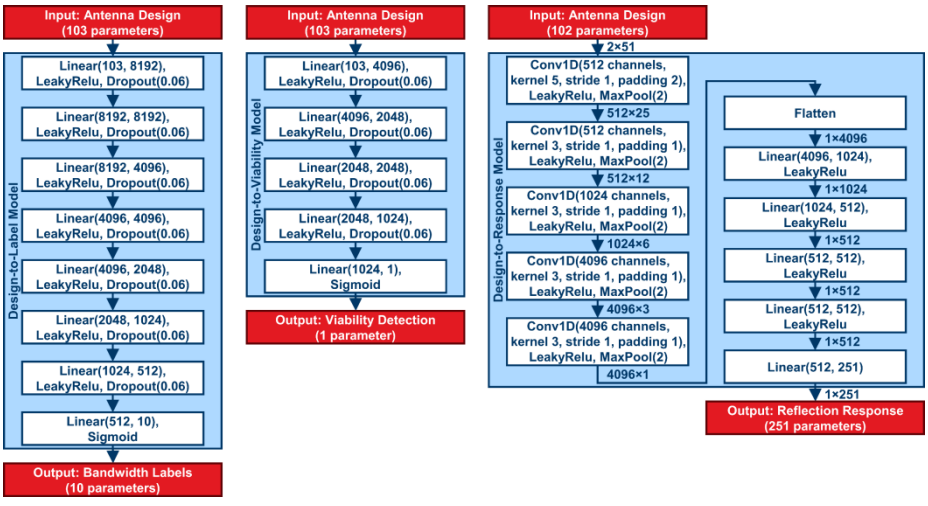


**Fig. 4.** Structures of the Design-to-Label, Design-to-Viability and Design-to-Response models.

ICCS Camera Ready Version 2026
To cite this paper please use the final published version:
DOI: 10.1007/978-3-032-29921-5_8

The 1Ddesign-to-Label-1.8.3 dataset, including classless samples (Section 4), was split into 90% training and 10% test subsets. A 10-fold CV was performed, and the model with the lowest validation loss was evaluated on the test set. Multiple hyperparameter settings were explored via grid search. Model hyperparameters are in Fig. 4, and learning parameters in Table 1. The model achieved a test accuracy of 0.926.

## 8 Label Classifier

The Design-to-Label model is an MLP serving as a multi-label classifier for antenna operating ranges [37]. It takes a design vector as input and outputs a 10-bit label vector indicating sub-bands (0.5 GHz each within 3–8 GHz) where the optimized antenna can operate. A label is assigned when the reflection coefficient and relative bandwidth criteria (Section 4) are satisfied. In the workflow, this model is used in step five to verify if the generated design is classified consistently with the condition vector. Unlike [43], where this model was used as a standalone evaluator, in the proposed framework it serves as one component of a broader multi-stage evaluation mechanism, contributing to intermediate verification rather than final decision-making.

The 1Ddesign-to-Label-1.8.3 dataset (Section 4) was split into 90% training and 10% test subsets. A 10-fold CV was used, and the model with the lowest validation loss was evaluated on the test set. Model hyperparameters are in Fig. 4, and learning parameters in Table 1. More details on the model are provided in [37].

The per-label test accuracies ranged from 0.917 to 0.966, decreasing with frequency. The macro-average accuracy reached 0.935, while the corresponding precision, recall, specificity, and F1 score were 0.768, 0.756, 0.964, and 0.761, respectively.

## 9 Response Estimator

The Design-to-Response model is a 1D CNN estimating antenna reflection response via regression. It takes a 2×51 tensor of x- and y-coordinates, where the first pair defines the feed point and the remaining 50 are vertices. The output is a 251-sample vector of $20 \cdot \log_{10}(|S_{11}(f)|)$ for 3–8 GHz in 20 MHz steps. A crucial step is data standardization (z-score) using the mean and standard deviation. Data are z-score standardized: inputs per coordinate channel, outputs per frequency.

The 1Ddesign-to-Response-2.8 dataset was split into 90% training and 10% test subsets. Bayesian optimization (BO) was applied to the training data to determine optimal structural and learning hyperparameters. The best configuration was validated using 10-fold CV to ensure a robust performance and reduce variance. The model with the lowest validation loss was evaluated on the test set, unused during BO and CV. Optimal model hyperparameters are in Fig. 4, and learning parameters in Table 1.

The model achieved a Mean Squared Error (MSE) of 3.789 $(\text{dB})^2$, a Mean Absolute Error (MAE) of 0.902 dB, a coefficient of determination ($R^2$) of 0.437, and a Root Mean Squared Error (RMSE) of 1.947 dB on the entire test set. It performs best below 6 GHz, where MAE < 0.62 dB and RMSE < 1.43 dB, peaking at 4.5 GHz. Above 6.5 GHz, performance declines but remains satisfactory overall.

ICCS Camera Ready Version 2026
To cite this paper please use the final published version:
DOI: 10.1007/978-3-032-29921-5_8

## 10 Results

It is important to note that the proposed framework is a design generator, not a predictive model. Therefore, the results reported in this section do not measure prediction accuracy of ML models, but rather the effectiveness of the generation process. To assess this, all generated designs were evaluated using full-wave EM simulations, which serve as the ground truth. The reported metrics quantify how often the generated designs satisfy the target operational sub-band conditions.

After training all models, an end-to-end pipeline (Section 3) was built to generate pseudorandom high-complexity antenna designs for a specified frequency range. For each sampling method (Section 5), 5,000 designs were generated, with 1,000 samples per sub-band. These designs underwent full-wave EM simulations in CST Microwave Studio [39] using the Finite Integration Technique [4–6]. The resulting reflection responses were analyzed, and bandwidth labels were generated. The obtained labels were compared with the conditioning labels, allowing quantitative evaluation of the generative pipeline's performance in producing designs matching the conditions.

Table 2 presents the results, including exact-match accuracy, relaxed-match accuracy, and macro-average metrics: accuracy, precision, recall, specificity, and F1 score, with 95% confidence intervals (CI) in parentheses. Macro-average accuracy reflects average correctness across sub-bands. Exact-match accuracy requires a perfect match between predicted and true labels, making it an overly strict metric. Relaxed-match accuracy is less restrictive, counting a match as correct if all active target labels are predicted, even with extra active sub-bands. This is more suitable for antenna design, as designs covering a superset of desired sub-bands remain valid for optimization.

The convex interpolation sampler enhances design diversity and achieves the best overall performance, with a relaxed-match accuracy of 0.769, a macro-average accuracy of 0.947, and a macro-average F1 score of 0.756. The high relaxed-match accuracy and F1 indicate that generated antennas meet target conditions and often cover broader frequency ranges, making them strong candidates for further optimization.

Table 3 shows per-label metrics. The generator shows highest consistency with conditions at lower frequencies (up to 6.0 GHz). Performance gradually declines with increasing frequency, with a noticeable drop in the highest sub-band (7.5–8.0 GHz).

**Table 2.** Overall experimental results.

| Latent sampling method | Posterior samples | Linear interpolation | Convex interpolation |
|---|---|---|---|
| exact-match accuracy | 0.577 (0.564–0.591) | 0.630 (0.616–0.643) | 0.634 (0.621–0.648) |
| relaxed-match accuracy | 0.701 (0.688–0.713) | 0.757 (0.746–0.769) | 0.769 (0.758–0.781) |
| macro-average accuracy | 0.940 (0.938–0.942) | 0.947 (0.945–0.949) | 0.947 (0.945–0.50) |
| macro-average precision | 0.734 (0.723–0.749) | 0.766 (0.755–0.776) | 0.764 (0.754–0.775) |
| macro-average recall | 0.701 (0.688–0.713) | 0.757 (0.746–0.769) | 0.769 (0.758–0.781) |
| macro-average specificity | 0.967 (0.965–0.968) | 0.968 (0.967–0.970) | 0.967 (0.966–0.969) |
| macro-average F1 score | 0.709 (0.699–0.719) | 0.751 (0.741–0.761) | 0.756 (0.746–0.766) |

ICCS Camera Ready Version 2026
To cite this paper please use the final published version:
DOI: 10.1007/978-3-032-29921-5_8

**Table 3.** Per-label results for the convex interpolation sampler.

| Label [GHz] | 3–3.5 | 3.5–4 | 4–4.5 | 4.5–5 | 5–5.5 | 5.5–6 | 6–6.5 | 6.5–7 | 7–7.5 | 7.5–8 |
|---|---|---|---|---|---|---|---|---|---|---|
| accuracy | 0.978 | 0.969 | 0.971 | 0.966 | 0.960 | 0.946 | 0.940 | 0.945 | 0.930 | 0.871 |
| precision | 0.985 | 0.858 | 0.896 | 0.839 | 0.826 | 0.744 | 0.740 | 0.719 | 0.609 | 0.426 |
| recall | 0.788 | 0.824 | 0.806 | 0.812 | 0.760 | 0.698 | 0.614 | 0.732 | 0.826 | 0.832 |
| specificity | 0.999 | 0.985 | 0.990 | 0.983 | 0.982 | 0.973 | 0.976 | 0.968 | 0.941 | 0.876 |
| F1 score | 0.876 | 0.841 | 0.848 | 0.825 | 0.792 | 0.720 | 0.671 | 0.725 | 0.701 | 0.564 |

**Table 4.** Average design generation time and algorithm iteration counts.

| Metric | Mean (95% CI) |
|---|---|
| Total time [s] | 0.703 (0.673–0.734) |
| Iterations | 30.105 (28.187–32.050) |
| Reiterations due to non-simple designs | 1.883 (1.741–2.029) |
| Reiterations due to nonviable designs | 12.286 (11.190–13.383) |
| Reiterations due to mismatched labels | 7.228 (6.693–7.780) |
| Reiterations due to mismatched responses | 7.708 (7.343–8.092) |

As shown in the Section 3, the algorithm operates iteratively. Each generated design is verified for geometry, viability, label consistency, and reflection compliance (Sections 7–9). Failed designs are rejected and regenerated until all criteria are met. Table 4 reports the average number of iterations and rejection causes, as well as the mean generation time of 0.703 s for the full end-to-end process, measured on a workstation with an Intel i7-12700 CPU, 32 GB RAM, and an RTX 3070 Ti GPU.

## 11 Conclusions

The proposed framework enables fully automated generation of complex antenna geometries conditioned on the target frequency bands, reducing expert bias and design time. The system integrates a CVAE with auxiliary MLP and CNN models for consistency verification. Auxiliary models remove the need for full-wave simulations while maintaining high predictive accuracy. The resulting low-latency process supports rapid design-space exploration and candidate selection for optimization.

It achieved exact-match accuracy of 0.634, relaxed-match of 0.769, macro-average accuracy of 0.947, and F1 of 0.756, with an average generation time of 0.703 s per design. Performance degradation occurs at higher frequencies (7.5–8.0 GHz). The process requires about 30 iterations per valid sample, indicating many generated designs are rejected due to infeasibility or label mismatch.

Future work will focus on BO of key pipeline models to improve conditional consistency and reduce rejection rates. In parallel, a new ML model will be developed for automated post-generation refinement of resonance characteristics.

ICCS Camera Ready Version 2026
To cite this paper please use the final published version:
DOI: 10.1007/978-3-032-29921-5_8

**Disclosure of Interests.** The author has no competing interests to declare that are relevant to the content of this article.

## References


1. Bandler, J.: Space Mapping-Have You Ever Wondered About the Engineer's Mysterious "Feel" for a Problem? [Speaker's Corner]. IEEE Microwave. 19, 112–122 (2018). https://doi.org/10.1109/MMM.2017.2780722.
2. Mroczka, J.: The cognitive process in metrology. Measurement. 46, 2896–2907 (2013). https://doi.org/10.1016/j.measurement.2013.04.040.
3. Ghassemi, M., Bakr, M., Sangary, N.: Antenna design exploiting adjoint sensitivity-based geometry evolution. IET Microwaves Antenna & Prop. 7, 268–276 (2013). https://doi.org/10.1049/iet-map.2012.0374.
4. Bekasiewicz, A., Kurgan, P., Koziel, S.: Numerically Efficient Miniaturization-Oriented Optimization of an Ultra-Wideband Spline-Parameterized Antenna. IEEE Access. 10, 21608–21618 (2022). https://doi.org/10.1109/ACCESS.2022.3152736.
5. Bekasiewicz, A., Dzwonkowski, M., Dhaene, T., Couckuyt, I.: Specification-Oriented Automatic Design of Topologically Agnostic Antenna Structure. In: Franco, L., De Mulatier, C., Paszynski, M., Krzhizhanovskaya, V.V., Dongarra, J.J., and Sloot, P.M.A. (eds.) Computational Science – ICCS 2024. pp. 11–18. Springer Nature Switzerland, Cham (2024). https://doi.org/10.1007/978-3-031-63759-9_2.
6. Bekasiewicz, A., Askaripour, K.: Performance Comparison of Automatically Generated Topologically Agnostic Patch Antennas. In: 2024 25th International Microwave and Radar Conference (MIKON). pp. 143–146. IEEE, Wroclaw, Poland (2024). https://doi.org/10.23919/MIKON60251.2024.10633953.
7. Ding, M., Jin, R., Geng, J., Wu, Q., Yang, G.: Auto-design of band-notched UWB antennas using mixed model of 2D GA and FDTD. Electron. Lett. 44, 257–258 (2008). https://doi.org/10.1049/el:20082056.
8. Trinh-Van, S., Yang, Y., Lee, K.-Y., Hwang, K.: A Wideband Circularly Polarized Pixelated Dielectric Resonator Antenna. Sensors. 16, 1349 (2016). https://doi.org/10.3390/s16091349.
9. Jacobs, J.P.: Accurate Modeling by Convolutional Neural-Network Regression of Resonant Frequencies of Dual-Band Pixelated Microstrip Antenna. Antennas Wirel. Propag. Lett. 20, 2417–2421 (2021). https://doi.org/10.1109/LAWP.2021.3113389.
10. Wu, G.-B., Zeng, Y.-S., Chan, K.F., Chen, B.-J., Qu, S.-W., Chan, C.H.: High-Gain Filtering Reflectarray Antenna for Millimeter-Wave Applications. IEEE Trans. Antennas Propagat. 68, 805–812 (2020). https://doi.org/10.1109/TAP.2019.2943432.
11. Bekasiewicz, A., Koziel, S., Plotka, P., Zwolski, K.: EM-Driven Multi-Objective Optimization of a Generic Monopole Antenna by Means of a Nested Trust-Region Algorithm. Applied Sciences. 11, 3958 (2021). https://doi.org/10.3390/app11093958.


ICCS Camera Ready Version 2026
To cite this paper please use the final published version:
DOI: 10.1007/978-3-032-29921-5_8

12. Whiting, E.B., Campbell, S.D., Mackertich-Sengerdy, G., Werner, D.H.: Dielectric Resonator Antenna Geometry-Dependent Performance Tradeoffs. IEEE Open J. Antennas Propag. 2, 14–21 (2021). https://doi.org/10.1109/OJAP.2020.3037826.
13. Lizzi, L., Viani, F., Azaro, R., Massa, A.: Optimization of a Spline-Shaped UWB Antenna by PSO. Antennas Wirel. Propag. Lett. 6, 182–185 (2007). https://doi.org/10.1109/LAWP.2007.894157.
14. Alroughani, H., McNamara, D.A.: The Shape Synthesis of Dielectric Resonator Antennas. IEEE Trans. Antennas Propagat. 68, 5766–5777 (2020). https://doi.org/10.1109/TAP.2020.2988984.
15. Alnas, J., Giddings, G., Jeong, N.: Bandwidth Improvement of an Inverted-F Antenna Using Dynamic Hybrid Binary Particle Swarm Optimization. Applied Sciences. 11, 2559 (2021). https://doi.org/10.3390/app11062559.
16. Koziel, S., Bekasiewicz, A.: Comprehensive Comparison of Compact UWB Antenna Performance by Means of Multiobjective Optimization. IEEE Trans. Antennas Propagat. 65, 3427–3436 (2017). https://doi.org/10.1109/TAP.2017.2700044.
17. Koziel, S., Bekasiewicz, A.: Multi-Objective Design of Antennas Using Surrogate Models. WORLD SCIENTIFIC (EUROPE) (2017). https://doi.org/10.1142/q0043.
18. Koziel, S., Ogurtsov, S.: Multi-Objective Design of Antennas Using Variable-Fidelity Simulations and Surrogate Models. IEEE Trans. Antennas Propagat. 61, 5931–5939 (2013). https://doi.org/10.1109/TAP.2013.2283599.
19. Koziel, S., Bekasiewicz, A.: Fast multi-objective design optimization of microwave and antenna structures using data-driven surrogates and domain segmentation. EC. 37, 753–788 (2019). https://doi.org/10.1108/EC-01-2019-0004.
20. Koziel, S., Bekasiewicz, A.: Domain segmentation for low-cost surrogate-assisted multi-objective design optimisation of antennas. IET Microwaves Antenna & Prop. 12, 1728–1735 (2018). https://doi.org/10.1049/iet-map.2017.0635.
21. Koziel, S., Bekasiewicz, A.: Multi-objective optimization of expensive electromagnetic simulation models. Applied Soft Computing. 47, 332–342 (2016). https://doi.org/10.1016/j.asoc.2016.05.033.
22. Yang, H., Zeng, R., Xu, G., Zhang, L.: A network security situation assessment method based on adversarial deep learning. Applied Soft Computing. 102, 107096 (2021). https://doi.org/10.1016/j.asoc.2021.107096.
23. Shen, S., Cai, C., Li, Z., Shen, Y., Wu, G., Yu, S.: Deep Q-network-based heuristic intrusion detection against edge-based SIoT zero-day attacks. Applied Soft Computing. 150, 111080 (2024). https://doi.org/10.1016/j.asoc.2023.111080.
24. Mohammadian, H., Ghorbani, A.A., Lashkari, A.H.: A gradient-based approach for adversarial attack on deep learning-based network intrusion detection systems. Applied Soft Computing. 137, 110173 (2023). https://doi.org/10.1016/j.asoc.2023.110173.
25. Shang, Y., Deng, W., Liu, J., Ma, J., Shang, Y., Dai, J.: Long term 5G base station traffic prediction method based on spatial-temporal correlations. Applied Soft Computing. 167, 112333 (2024). https://doi.org/10.1016/j.asoc.2024.112333.
26. Baz, A., Logeshwaran, J., Natarajan, Y., Patel, S.K.: Enhancing mobility management in 5G networks using deep residual LSTM model. Applied Soft Computing. 165, 112103 (2024). https://doi.org/10.1016/j.asoc.2024.112103.

ICCS Camera Ready Version 2026
To cite this paper please use the final published version:
DOI: 10.1007/978-3-032-29921-5_8

27. Panek, M., Pomykała, A., Jabłoński, I., Woźniak, M.: 5G/5G+ network management employing AI-based continuous deployment. Applied Soft Computing. 134, 109984 (2023). https://doi.org/10.1016/j.asoc.2023.109984.
28. Huang, J., Nan, J., Gao, M., Wang, Y.: Antenna modeling based on meta-heuristic intelligent algorithms and neural networks. Applied Soft Computing. 159, 111623 (2024). https://doi.org/10.1016/j.asoc.2024.111623.
29. Khan, M.M., Hossain, S., Mozumdar, P., Akter, S., Ashique, R.H.: A review on machine learning and deep learning for various antenna design applications. Heliyon. 8, e09317 (2022). https://doi.org/10.1016/j.heliyon.2022.e09317.
30. Shi, D., Lian, C., Cui, K., Chen, Y., Liu, X.: An Intelligent Antenna Synthesis Method Based on Machine Learning. IEEE Trans. Antennas Propagat. 70, 4965–4976 (2022). https://doi.org/10.1109/TAP.2022.3182693.
31. Ramasamy, R., Anto Bennet, M.: An Efficient Antenna Parameters Estimation Using Machine Learning Algorithms. PIER C. 130, 169–181 (2023). https://doi.org/10.2528/PIERC22121004.
32. Gao, J., Tian, Y., Chen, X.: Antenna Optimization Based on Co-Training Algorithm of Gaussian Process and Support Vector Machine. IEEE Access. 8, 211380–211390 (2020). https://doi.org/10.1109/ACCESS.2020.3039269.
33. Fu, H., Tian, Y., Meng, F., Li, Q., Ren, X.: Microstrip antenna modelling based on image-based convolutional neural network. Electronics Letters. 59, e12910 (2023). https://doi.org/10.1049/ell2.12910.
34. Zheng, X., Meng, F., Tian, Y., Zhang, X.: Design of monopole antennas based on progressive Gaussian process. Int. J. Microw. Wireless Technol. 15, 255–262 (2023). https://doi.org/10.1017/S1759078722000125.
35. Zhang, X., Tian, Y., Zheng, X.: Optimal Design of Fragment-Type Antenna Structure Based on PSO-CNN. In: 2019 International Applied Computational Electromagnetics Society Symposium - China (ACES). pp. 1–2. IEEE, Nanjing, China (2019). https://doi.org/10.23919/ACES48530.2019.9060460.
36. Cai, J., Zhong, R., Li, Y.: Antenna selection for multiple-input multiple-output systems based on deep convolutional neural networks. PLoS ONE. 14, e0215672 (2019). https://doi.org/10.1371/journal.pone.0215672.
37. Czaplewski, B.: Neural Network for Evaluating the Operational Range of Antennas with Randomly Generated Designs. In: Lees, M.H., Cai, W., Cheong, S.A., Su, Y., Abramson, D., Dongarra, J.J., and Sloot, P.M.A. (eds.) Computational Science – ICCS 2025. pp. 394–402. Springer Nature Switzerland, Cham (2025). https://doi.org/10.1007/978-3-031-97635-3_47.
38. Czaplewski, B.: 1Ddesign-to-label-1.8.3 - Antenna Designs with Operating Frequency Range Labels, https://zenodo.org/doi/10.5281/zenodo.14982974, (2025). https://doi.org/10.5281/ZENODO.14982974.
39. CST Microwave Studio, (2019).
40. Czaplewski, B.: 1Ddesign-to-response-2.8 - Free-Form Antenna Designs with Reflection Responses, https://zenodo.org/doi/10.5281/zenodo.16784875, (2025). https://doi.org/10.5281/ZENODO.16784875.

ICCS Camera Ready Version 2026
To cite this paper please use the final published version:
DOI: 10.1007/978-3-032-29921-5_8